

Article

A Passive, Skin-Attachable Multi-Sensing Patch Based on Semi-Liquid Alloy Ni-GaIn for Wireless Epidermal Signal Monitoring and Body Motion Capturing

Shipeng Lin, Jiming Fang, Tianchen Ye, Yan Tao, Shengshun Duan  and Jun Wu *

School of Electronic Science and Engineering, Southeast University, Nanjing 210096, China; linsp@seu.edu.cn (S.L.); cescfang@seu.edu.cn (J.F.); ytc1412@seu.edu.cn (T.Y.); taoyan@seu.edu.cn (Y.T.); 230218163@seu.edu.cn (S.D.)

* Correspondence: wujunseu@seu.edu.cn



Citation: Lin, S.; Fang, J.; Ye, T.; Tao, Y.; Duan, S.; Wu, J. A Passive, Skin-Attachable Multi-Sensing Patch Based on Semi-Liquid Alloy Ni-GaIn for Wireless Epidermal Signal Monitoring and Body Motion Capturing. *Electronics* **2021**, *10*, 2778. <https://doi.org/10.3390/electronics10222778>

Academic Editor: Gianluca Traversi

Received: 8 September 2021

Accepted: 10 November 2021

Published: 13 November 2021

Publisher's Note: MDPI stays neutral with regard to jurisdictional claims in published maps and institutional affiliations.



Copyright: © 2021 by the authors. Licensee MDPI, Basel, Switzerland. This article is an open access article distributed under the terms and conditions of the Creative Commons Attribution (CC BY) license (<https://creativecommons.org/licenses/by/4.0/>).

Abstract: Wearable integrated systems that rely on liquid metal commonly require an extremely complicated, high-cost fabrication process, while lacking multiple sensing functions without conductive wires connected to external electronic systems. A multi-sensing wearable patch independent from sophisticated manufacturing method and excessive use of wires has yet to be developed. Herein, we introduce a wireless, battery-free, and skin-attachable patch with multiple sensing capacities, utilizing a low-budget, less time-consuming and design-customizable fabrication method. In an effort to achieve our goal, the general sensing system architecture is promoted, which consists of a semi-liquid alloy Ni-GaIn based strain sensor and a co-designed near-field-communication (NFC) tag integrating thermistor, photoresistor, as well as sensor interface circuits, enabling energy-autonomous power supply and wireless data transmission. In human volunteers, the patch was mounted on the skin surface to demonstrate real-time temperature and light intensity signal monitoring. Further evaluation of body motion capturing involved finger bending and swallowing, demonstrating the feasibility of practical applications in different scenarios. Continuous and simultaneous multi-type signal sensing using the wearable patch should enrich the dimensions of measurements of body response to daily activities, unveiling the potential for remote human health monitoring, advanced human-machine interfaces, and other applications of interest.

Keywords: flexible; multi-sensing; semi-liquid alloy; wireless; passive; epidermal signal monitoring; motion capturing; NFC

1. Introduction

Wearable devices with adequate stretchability, as well as the capability of sensing various signals, are required to fulfill the needs for applications ranging from remote health monitoring [1] and personal diagnostics to body motion capture and human-machine interactions [2]. Recent studies have demonstrated the importance of integrating multiple sensors into a single device [3]. This concept of sensor integration has evolved towards the combination of diverse sensor modalities [4]. Recent efforts have led to the combination of physical, chemical, and biomedical signal sensing, which is realized in a single system with interface to human skin or organisms, including temperature, ion concentrations [5], glucose [6] and thermoregulatory sweat [7]. Meanwhile, it is no surprise that stretchable wearable devices have been targeted as a novel approach of human motion capture, such as finger bending, hand gesture recognition [8] and even sign-to-speech translation [9]. All these fantastic functions are based on the flexible sensor arrays enabling small deformation detection, which can be considered as an extensive way of signal acquisition and processing from the perspective of multiple sensing integration. However, to the best of our knowledge, it remains a systematic research of a comprehensive general multi-sensing device, which requires an appropriate fabrication method of flexible components, stretch-

able sensors, sensor interface circuits, memories, digital processing units, passive power supply and wireless data transmission.

Liquid metal Gallium-Indium alloy has been spotlighted as a potential material for flexible electronics due to its outstanding liquidity, high conductivity, excellent stretchability [10] and biocompatibility. The materials used in most existing flexible strain sensors are still graphene [11], carbon nanotubes [12], etc., but they are more prone to fracture and crack expansion when the sensor undergoes large-scale bending and deformation, due to the solid-state characteristics, thereby affecting the accuracy of the sensor.

Additionally, some metal composites have been explored to improve the adhesion of liquid metal to various substrates [13]. For instance, GaIn mixed with Cu [14] or Au [15] particles display better adhesion and less liquidity. Furthermore, many kinds of flexible electronic devices have been fabricated, such as strain sensors [16], stretchable antenna [17], bioelectrodes [18] and supercapacitors [19].

Meanwhile, different fabrication methods have been promoted to form circuit patterns, including the micro-channel injection method using lithography [20], thin film deposition using sputtering technique [21], and transfer printing using different substrates. There still exists an ongoing challenge of improving current fabrication approaches considering the trade-off among cost, complexity, reliability, customization, and reusability. As for advanced power source solutions, considerable research has been conducted in applications for piezoelectricity [22], triboelectricity [23], thermoelectricity [24], biofuel cells [25] and wireless power transfer [26]. On the other hand, integrating systems featuring wireless data transmission have been demonstrated with Bluetooth [27] and near-field-communication (NFC) technology [26]. To realize both battery-free and wireless functions, it is optimal to apply the NFC strategy for an ultra-low power consumption and high-accuracy multiple signals sensing integrated system.

In the present work, we report a lightweight, skin-attachable, biocompatible, and customizable patch integrating multi-sensing functions. Semi-liquid Ni-GaIn has been successfully prepared to lay the foundation of flexible strain sensor owing to thorough study of GaIn mixing with Ni particles. By utilizing the significant adhesion selection of Ni-GaIn on PET and silicone gel, we promoted a newly fast fabrication method, which we called it Direct Printing Using Laser Engraved Masks (DPULEM), with key advantages of low cost, high accuracy, customization, and excellent reusability. A serpentine structured flexible strain sensor is combined with a co-designed sandwich-architecture NFC tag, which assembles thermistor and photoresistor and exhibits as sensor interface circuits, to implement the complete design of wearable patch. The system communicates with an external NFC reader in a wireless fashion via inductive antenna to enable power harvesting and data transmitting within a maximum distance of 8 cm. The patch can be mounted on any part of human skin to offer the ability of epidermal temperature and light intensity sensing with negligible delay and long-term monitoring. Meanwhile, the patch is able to capture real-time body motion with the index finger bending and swallowing as examples. The results demonstrate that our fully wireless, battery-less integration design as well as fast, hybrid implementation of the wearable patch shows great potential in remote human health care, body gesture configuration, human-machine interaction, and other relevant areas.

The article is arranged as follows. In Sections 2.1 and 2.2, we demonstrated the fabricated methods and characterization results of liquid metal materials and strain sensors; in Section 2.3, the NFC system used to provide wireless power supply and data transmission and related application examples were presented; in Section 3, we made a summary of our work. Finally, in Section 4, the detailed experimental methods were discussed.

2. Results and Discussion

2.1. Characterization of the Semi-Liquid Alloy Ni-GaIn

The electrical resistance was measured with a digital multimeter [14150 SW Karl Braun Drive PO Box 500 Beaverton, OR 97077,2400, Keithley, OH, USA] with copper wires

inserted into both ends of Ni-GaIn microchannels. For Ni-GaIn traces with 1 mm width and 5 cm length, the average electrical resistance value was $1.2 \Omega (\pm 0.1 \Omega)$, which enabled Ni-GaIn lines with adequate conductivity to provide reliable electrical connections for discrete components.

In the present work, we introduced an agile manufacturing method to fabricate flexible strain sensors in different shapes, called direct printing using laser engraved masks (DPULEM), as shown in Figure 1. The circuit pattern of the strain sensor was initially designed with engraving parts highlighted in CAD software. Then, the design file was imported into a special software controlling the laser engraver, as shown in Figure S1. Here, we used a thin film of polyethylene terephthalate (PET) [Shanghai Ruizhi Industrial Co., Ltd., Shanghai, China] with a thickness of 0.1 mm as mask's material, as shown in Figure S2. The two engraving machine parameters, speed and power were set as 10% and 40%, respectively. It required 7 min on average to fabricate the mask we needed for DPULEM, with time increasing in proportional to the design complexity. Then, the prepared mask was placed onto the silicone gel substrate and the Ni-GaIn droplets were uniformly roll printed to the substrate using a metal roller (Yunlong District Lu Rui hardware firm, Xuzhou, China) through the engraved parts of the mask. Finally, we obtained a self-designed flexible strain sensor after removing the mask from the substrate.

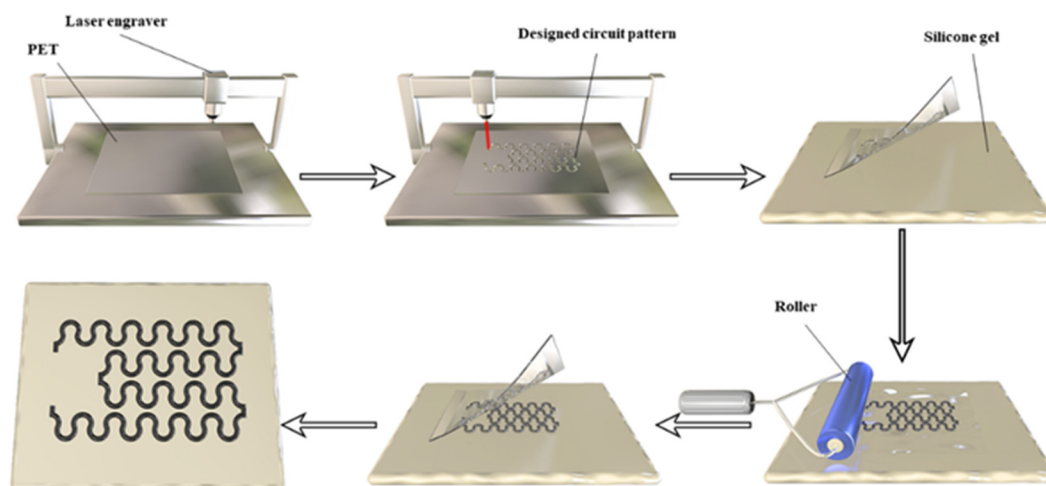


Figure 1. The flow chart of the Direct Printing Using Laser Engraved Masks (DPULEM) method.

The mechanism of how mixing ratio of Ni micro particles changed the properties of Ni-GaIn was studied to reach better fabrication performance of DPULEM method with higher accuracy and more stability. Recent studies [10] have reported that mixing GaIn alloy with solid-state metal particles, including nickel and copper, would reduce the alloy's liquidity due to the metal oxidation produced in this process. Figure 2a shows a series of photographs of Ni-GaIn printed on silicone gel substrate, with mixing ratios of Ni micro particles ranging from 0 to 10% in the step length of 2%. It was observed that the surface roughness of the semi-liquid alloy significantly increased with the content of Ni micro particles, which was in an agreement with previous research results. Before stirring, the solid Ni microparticles were floating on the surface of liquid GaIn as two separate systems due to the high surface tension of the liquid alloy and the blockage of the gallium oxide layer. With continuous stirring, Ni micro particles were gradually internalized as being wrapped by the gallium oxide layer until completely soaked into the GaIn to form the semi-liquid Ni-GaIn system. Through this process, it was demonstrated that the addition of Ni microparticles wrapped up by gallium oxide layer reduced the surface tension and liquidity of GaIn.

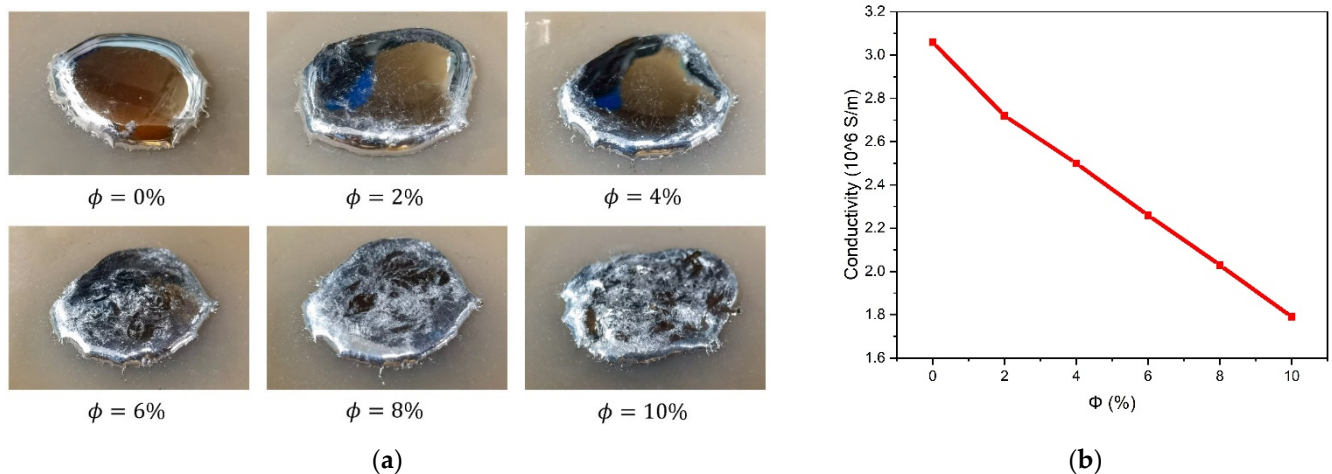


Figure 2. (a) Photographs of Ni-GaIn on silicone gel substrate with different mixing ratios of Ni micro particles; (b) Change of conductivity with increasing ϕ .

In general cases, properties of Ni-GaIn changed with different mixing ratios of Ni micro particles (ϕ). It should be noted that the composition content of Ni micro particles ranged from 0 to 10%. The mixing ratio was defined as $\phi = m_{\text{Ni}}/m_{\text{GaIn}}$, where m_{Ni} and m_{GaIn} represented the mass of the Ni particles and the GaIn alloy, respectively. In particular, we set ϕ to be 6% for the best performance of Ni-GaIn when fabricating customized circuits on stretchable substrates including silicone gel. For semi-liquid Ni-GaIn with ϕ more than 10%, it was unable to form a continuous conductive line as Ni-GaIn gathered into droplets due to its relative high surface tension. In cases where ϕ was more than 6%, Ni-GaIn showed more solid-state characteristic of the semi-liquid as it could be evenly printed on silicone gel using DPULEM method. Besides, the conductivity of Ni-GaIn decreased with ϕ increasing, as shown in Figure 2b. Considering the trade-off between liquidity and conductivity of Ni-GaIn, Ni-GaIn with $\phi = 6\%$ was used in DPULEM method to achieve the most stable printing performance.

It was fundamental for the implementation of DPULEM that Ni-GaIn had outstanding adhesion selection on the surface of silicone gel and polyethylene terephthalate (PET). A simple experiment was conducted to show the adhesion selection of Ni-GaIn to the surface of PET and silicone gel, which demonstrated the practicability of DPULEM. A pressure of around 0.098 N was applied to the Ni-GaIn droplets using a metal block (weight of 10 g). Then, we observed the contact angle of Ni-GaIn on each substrate using an optical microscope. The results of the contact angle test revealed the contact angles of Ni-GaIn droplets on silicone gel and PET were 97° and 150° , respectively. The far smaller contact angle on the surface of silicone gel explained absolute better adhesion with Ni-GaIn droplets than PET, demonstrating the practicability of using silicone gel and PET as substrate and mask separately in DPULEM method.

2.2. Characterization of Flexible Strain Sensors in Different Shapes

In order to make the resistance change of the strain sensor sensitive to uniaxial tensile strain, the strain sensor is usually composed of several longitudinal sections connected by short transverse segments with large cross area [28]. By following this principle, we fabricated strain sensors of four extended design approaches, as shown in Figure 3, based on the wavy structure using the DPULEM method, which were described as shamrock, serpentine, streamline and periodic U shape architecture, respectively.

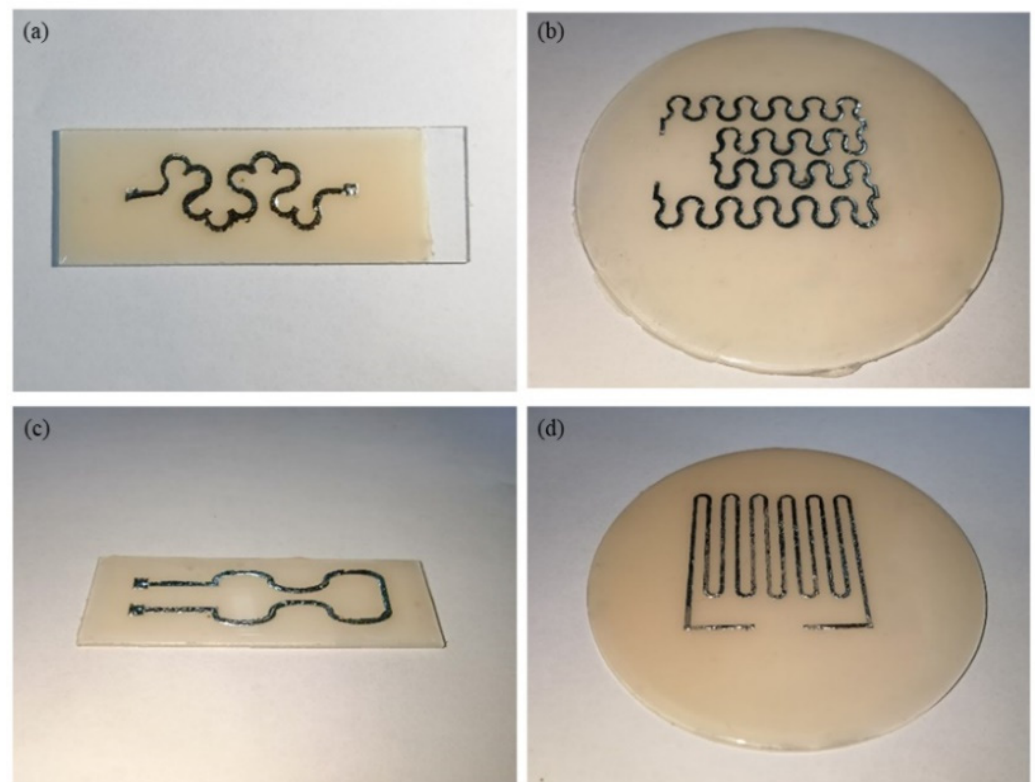


Figure 3. Circuit patterns of strain sensor in different wavy structures: (a) shamrock; (b) serpentine; (c) streamline; (d) periodic U shape.

To compare the stretchability of these four structures, tensile test experiments with normalized length change ranging from 0 to 50% were conducted to show the differences of their response of electrical resistance change. Mechanical characteristic evaluation of the sensor was performed with a professional uniaxial stretcher [TST-01 H, Jinan Zhongce Electromechanical Equipment Co. Ltd., Jinan, China], which was shown in Figures S3 and S4. During the stretching process, the electrical resistance was monitored with the digital multimeter with copper wires inserted into both ends of Ni-GaIn microchannels. After a testing cycle, we obtained a series of discrete data illustrating how the impedance varied as the strain sensor stretching and recovering, with relative uniaxial strain applied along the sensor plane ranging from 0 to 50%.

Figure 4a,b illustrated the experiment results with four curves based on discrete data points. Different structured sensors had good linearity under small deformation, and with the exception of the streamline-shaped sensor, the R^2 of the other three sensors exceeded 0.99 within the deformation range of 0–20%. As the normalized length change approaching 50%, there existed a sudden rise in both streamline-shape and shamrock-shape curves, which indicated unexpected cracking inside the semi-liquid traces. It demonstrated that these two structures rendered the sensor promising stretchability only within a limited small strain range as they were not able to preserve reversible and elastic response against large deformations. As for serpentine and periodic U shape structures, they both maintained stable electrical characteristics with linearity in resistance change under extreme tensile strain. In terms of sensitivity, the streamline structured strain sensor showed the highest sensitivity, but it did not perform well in terms of linearity and stability, which may be due to its simple structure.

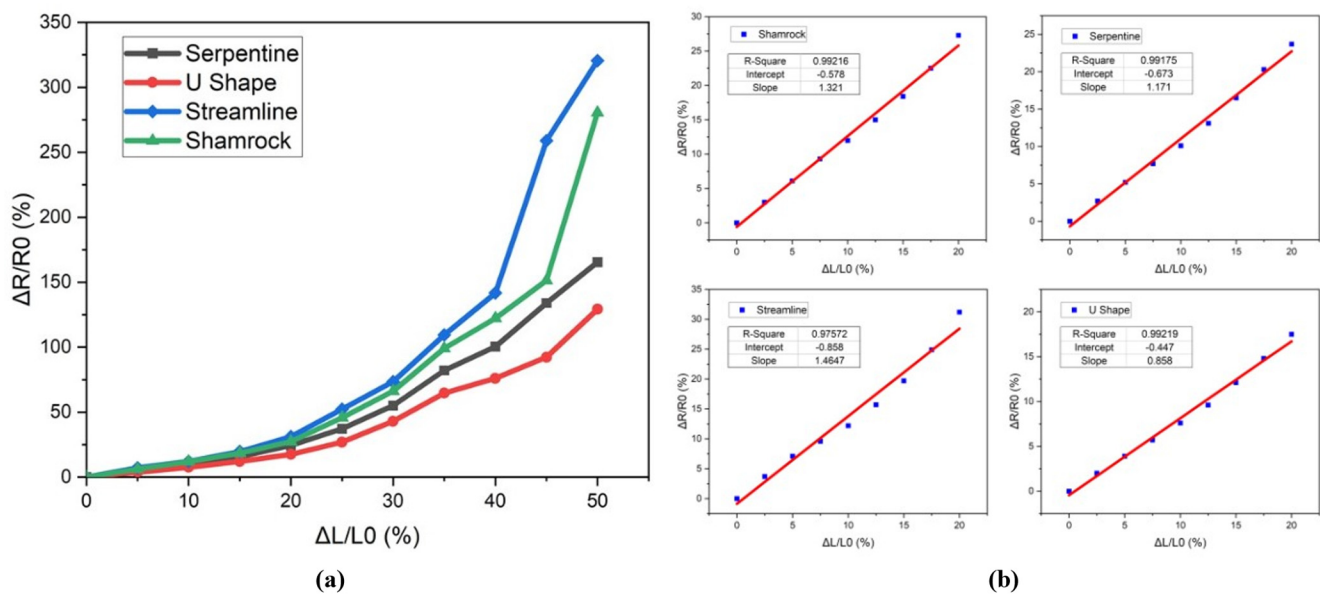


Figure 4. (a) Comparisons of four various structured sensors under same dynamic loading; (b) Linear fitting results of four different shapes of sensors when the deformation variable is between 0–20%.

Figure 5a illustrated how the normalized change of resistance ($\Delta R/R_0$) responded to applied uniaxial strain which presents as normalized change of length ($\Delta L/L_0$). The value of resistance change was collected in a typical stretch-recover cycle with $\Delta L/L_0$ ranging from 10 to 50%. Three pairs of curves with different hysteresis represented characteristics for these three types of strain sensors with higher sensibility. For streamline and shamrock structured sensors, change of resistance in the stretching process obviously did not overlap with that in the recover process during its stretch-release cycle, introducing a large hysteresis in the response. It could be observed that the release curves gradually separated from the stretch curves as the release process proceeded when they left the start point of recovering, which led to an enormous increase in resistance (85% for the shamrock-shape and 270% for the streamline-shape) when they went back to their original points after a stretch-recover cycle. The phenomena revealed internal crack and fracture of Ni-GaIn traces on silicone gel layer. In contrast to these two sensors, there existed literally no difference (less than 10% even under extreme conditions) for the two curves representing stretch and release in the case for serpentine structured sensor, suggesting reversible behavior for this kind of flexible strain sensor. The excellent resistance recoverability and negligible hysteresis of serpentine structure could be due to the circuit pattern design which accommodate uniaxial stretch-release with overall response in periodic wave-structure dealing with the internal fracture Ni-GaIn traces under frequent stretching.

We tested the serpentine structured sensor for 100 stretch-release cycles under 30% strain, which was performed at a dynamic loading frequency of 10 s per cycle. Figure 5b presents the results of the last 10 cycles, where the serpentine sensor remained stable electrical properties. The resistance was fully recovered for most stretch-release cycles and presented negligible hysteresis after a great number of stretching. The results demonstrated the strain sensor formed in serpentine structure with excellent durability under repeat testing, showing great potential of reliable performance in practical applications featuring long-term monitoring.

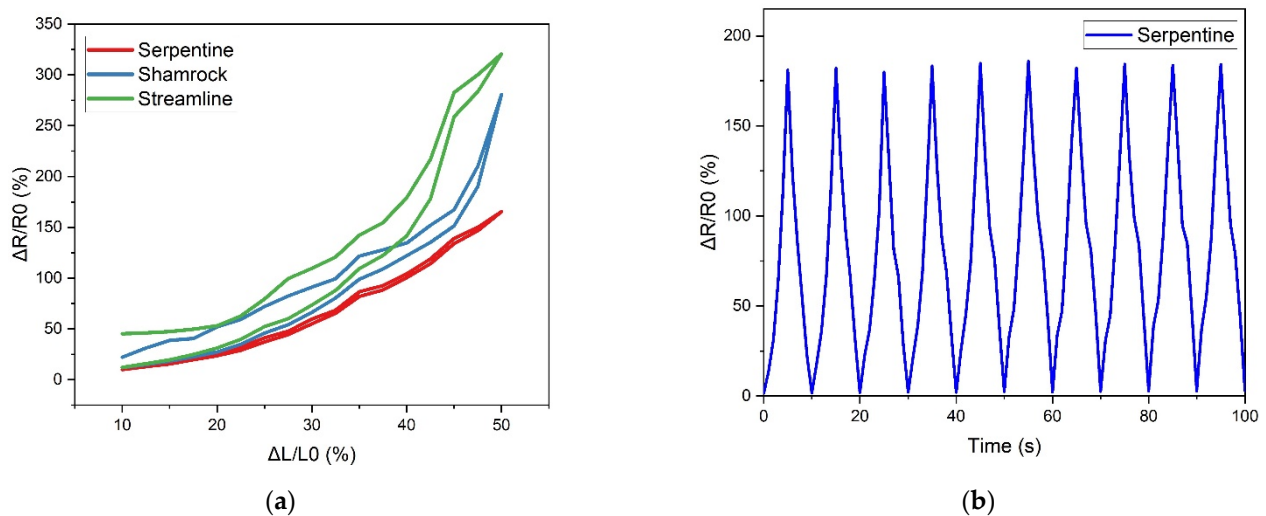


Figure 5. (a) Hysteresis curve for the streamline, shamrock and serpentine structured sensors; (b) response of the serpentine structured strain sensors for the last 10 out of 100 stretch-release cycles.

Wavy structures absorbed compressive and tensile strains with changes in wave lengths and amplitudes instead of potential destructive strain in the bulk of stretchable materials [28]. Therefore, applying wavy structure enabled semi-liquid Ni-GaIn traces adequate stretchability to avoid material fractures while maintaining promising conductivity. In general, the serpentine structure has linear resistance change, negligible hysteresis, and excellent durability under various strain, which is attributed to the device's electrical-mechanical robustness. After comprehensive considering of linearity, sensitivity and stability, serpentine structure was chosen to be our novel approach of wavy structure for the strain sensor that we used to compose our wearable multi-sensing patch. For the serpentine structured strain sensor shown in Figure 3, its geometric dimensions were 51.9 mm in length, 40.5 mm in width, and 0.1 mm in height, and the width of the liquid metal trace was 1.2 mm.

2.3. Characterization of the Wearable Multi-Sensing Patch

To perform multiple sensing functions on skin surface wirelessly, the full multi-sensing patch was constructed with a customized flexible strain sensor and a co-designed NFC tag, as shown in Figure 6a. For the fabrication of this NFC tag, as shown in Figure S5, an Si-based logic bare die [RF430FRL152H, Texas Instruments, P.O. Box 660199, Dallas, Texas 75266-0199, TX, USA] near field communication (NFC) chip was integrated with the copper antenna, regular resistors, capacitors, and a thermistor as well as a photoresistor. The tag structure was designed as a three-layer sandwich, which was implemented as a polyimide (PI) layer with two copper layers stacked on both sides of it. The antenna was embedded in the ultra-thin copper layer, while the passive components were soldered on preserved pads with the thermistor mounted on the side closer to the skin. The electrical interconnections, antenna and pads were fabricated with chemical vapor deposition (CVD) process. Both ends of the flexible strain sensor were electrically connected to the terminals of the sample channel of the analog-to-digital convertor (ADC) integrated in the NFC chip using conductive silver adhesives, while thermistor and photoresistor were soldered to connect. The strain sensor combined with the NFC tag was placed on the silicone gel substrate as a whole system. We added the same amount of each type of liquid Ecoflex separately into a beaker, stirred the mixture and poured it onto the device slowly and evenly. The full multi-sensing patch was completely produced after the Ecoflex was cured to naturally formed a thin film as encapsulation.

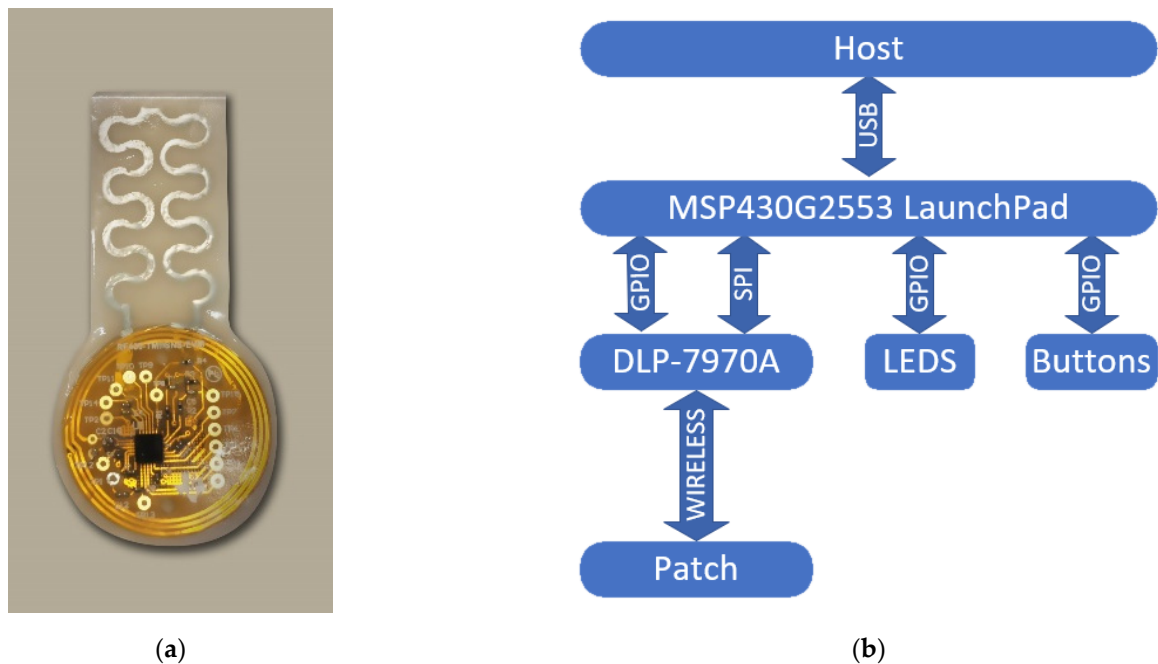


Figure 6. (a) Packaged skin-attachable multi-sensing patch; (b) Block diagram of the NFC card reader system working pattern.

To monitor epidermal signals and capture body motions, the customized patch was mounted on the skin of a specific part of the human body. As shown in Figure S6, a near-field-communication (NFC) reader, consisting of a host board [MSP430G2553, Texas Instruments, USA] and an NFC reader module [DLP7970A, Texas Instruments, USA], which working pattern was shown in Figure 6b, was used for power acquisition and data transmission. The passive reader module was electrically interconnected to the host board via pre-designed terminals and communicated with each other via serial peripheral interface (SPI). The host board was connected to PC laptop with a USB wire to transmit collected data simultaneously via the serial port of universal asynchronous transceiver (UART). The patch functioned well at an average distance within 8 cm (due to power consumption of the NFC reader and size of the antenna) from the antenna embedded in the reader module.

Then, the patch can be wirelessly powered by and communicate with the external reader via the magnetic inductive coupling coils (antenna) at a resonance frequency of 13.56 MHz. The NFC tag was designed to resonate at around 13.56 MHz by appropriately setting the capacitance value of the tuning capacitor connected in parallel with the inductor antenna electrically, which jointly formed a required LC resonant circuit. Alternating current (AC) power transferred from the antenna embedded in the reader to that of the NFC tag was rectified by the NFC chip to provide energy supply for proper operation of ADC, temporary data storage in FRAM and data transmission speed of 384 bits per second. For NFC chip to work properly, necessary peripheral components, such as resistors and capacitors, were applied to compose the NFC tag, including decoupling capacitors to eliminate self-excitation as well as to reduce current noise, bypass capacitors to filter out ripple voltage and a reference resistor for ADC calibration.

To realize the multi-sensing task, the flexible strain sensor, as well as thermistor and photoresistor, plays a role as variable resistor with both ends electrically connected to the terminals of the sample channel of ADC. If variable resistor sampling is chosen, the NFC chip emits a small current (approximately 2.4 μA) through the reference resistor and variable resistor pins, which creates a voltage on the positive side of them. This voltage is then sampled by the ADC. With known resistor value and the raw ADC sample data, the accurate current being emitted can be calculated. Then, the resistance value of the

variable resistor can be calculated because the current through both is the same. The value of related physical signal can be calculated or converted numerically according to the function of resistance change by corresponding physical signal. The device stores the ADC value directly after sampling and the calculations must be done externally. Raw data is continuously transmitted to the external reader at a sampling rate of 24 Hz.

To monitor the wireless epidermal signal, the patch was attached onto surface of human skin. As shown in Figure 7a, the temperature value was measured with patch placed on forehead, which fluctuated slightly around 33.2 °C. The results exhibited identical views with regular behavior of body surface temperature. By applying the same method, Figure 7b illustrated the intensity of light shed on the back of hand with a sudden block of opaque object under a fluorescent lamp indoors. The appearance of a distinguishable wave valley justified that the multi-sensing patch responded to the change of light intensity around the skin rapidly with hardly any delay and with sufficient acquisition of the signal.

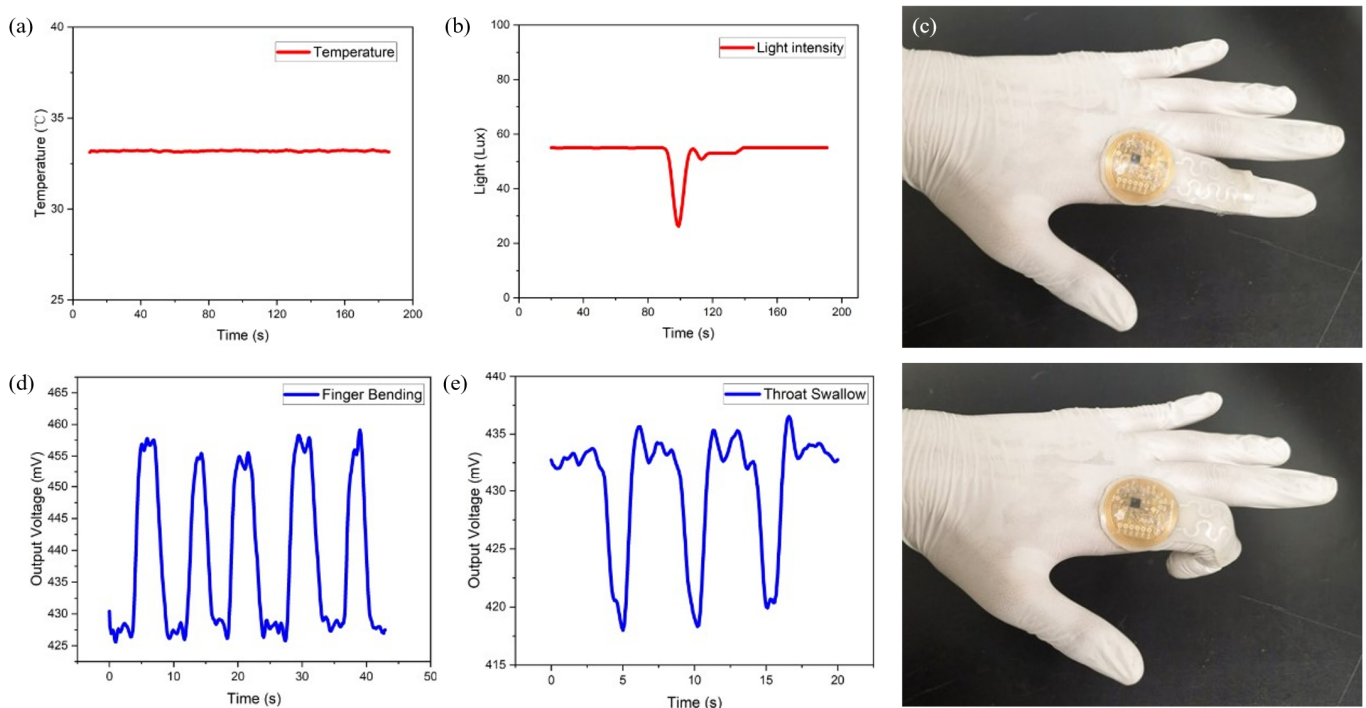


Figure 7. Epidermal signal monitoring of (a) temperature and (b) light intensity; (c) Illustration of real-time motion detection with wearable patch attached to the joint of index finger; Motion detection of (d) index finger bending and (e) swallowing.

As an example of demonstrating motion capture function of the multi-sensing patch, the device was mounted on the joint of the index finger to obtain data simultaneously while straightening and bending the index finger, as shown in Figure 7c and Figure S7. Due to the resistance change proportional to the tensile strain, the output data could be characterized with time-variant voltage since the emitting current of sample channel was constant. Each straightening–bending motion of the index finger would be illustrated as a wave peak or a voltage pulse. Figure 7d showed how the multi-sensing patch represented two distinguishable straightening–bending motions wirelessly, which verified our designed implementation. Swallow was another trickier motion captured by our multi-sensing patch, since the deformation of the device was ultra-small, while swallowing and the surface with bumping was difficult to attach to, owing to the pomum adami. Figure 7e recorded the change in output voltage while swallowing, where concave peaks represented unique response of irregular deformation detected by the strain sensor embedded in the multi-sensing patch.

3. Conclusions

Impressively, we paved a new way to endow a wearable patch with multi-sensing functions, implement it with an agile fabrication method DPULEM based on semi-liquid alloy Ni-GaIn and enable its wireless and passive features by applying NFC technology. The multi-sensing patch consisted of a serpentine structured flexible strain sensor that detected small deformation and an NFC tag integrating thermistor and photoresistor, which was in charge of power harvesting, signal processing and data transmission. The circuit patterns of flexible strain sensor were obtained by applying DPULEM process with key advantages including stable fabrication performance, low cost, customized design, and high efficiency compared to other strategies. Cases for variable sensing capacities integrated in our patch were epidermal signal measurement including temperature and light intensity. Finger flexion and swallow were demonstrated as examples of body motion capturing using this system.

However, our work has certain limitations. On the one hand, our patch can only perform energy acquisition and data transmission normally within the range of 8 cm from the NFC reader, due to the nature of RF430FRL152H. On the other hand, the patch we fabricated is not completely flexible, and there will still be rigid components such as resistors and capacitors on the NFC tag, which needs to be placed in a relatively flat place with less deformation during the working process, so as not to affect the performance of the antenna.

The results have shown that we have unlocked the critical bottleneck of the trade-off among difficulties of sensor design customization, complexity of fabrication method and combination of wireless and passive processing system. The lightweight, skin-attachable patch represents effective power consumption with excellent stretchability and provides insights into integration of high-accuracy multi-type epidermal signal monitoring and automatic real-time body motion detection in a single platform. It thus opens the way to a series of skin-conformal devices capable of sensing various information simultaneously regarding the status of human health, which provides a first step towards next-generation wearable patches featuring hybrid signals processing with extensive applications in remote health care, high-quality human motion reconfiguration and human-machine interaction.

4. Experiment Section

4.1. Preparation of Semi-Liquid Alloy Ni-GaIn

The liquid metal GaIn chosen in this paper was provided by Dongguan Dingguan Metal Technology Co., Ltd. (99.9% purity). Gallium-Indium alloy consisted of 75.0 wt% gallium and 25.0 wt% indium, with low melting point (16 °C) and low electrical resistivity ($2.94 \times 10^{-7} \Omega \cdot \text{m}$). Nickel microparticles (99.5%) needed were purchased from Shanghai Macklin Biochemical Co., Ltd.

The gallium (75.0 g) was firstly added to a beaker, and then heated in the water bath at 60 °C [11] until it was melted. Next, the indium (25.0 g) was put into the melted gallium. Then, the Ga-In liquid mixture was kept at 80 °C for 1 h with continuous stirring to be mixed evenly and completely. Later, a certain amount of Nickel particles was added in the GaIn alloy. The solid-liquid mixture was vigorously agitated using a glass bar for another 10 min until the Ni particles were totally swallowed by GaIn alloy. Finally, we obtained the GaIn alloy mixed with Ni particles, which is called Ni-GaIn semi-liquid alloy.

4.2. Fabrication of Flexible Strain Sensor on Silicone Gel Substrate

The liquid silicone gel used as the printing substrate was purchased from Hong Ye Jie Technology Co., Ltd, Shenzhen, China. It was composed of 50.0 vol% A-type and 50.0 vol% B-type silicone gel. We added 3 mL of each type of silicone gel separately into a beaker, stirred the mixture for 30 s and carefully placed it onto the center of the ultra-clean surface of a glass slide located on a spin coater. The rotation speed and the spin coating duration were optimized to be 200 RPM and 50 s, respectively. Then, we obtained a round flexible substrate with a radius of 6 cm.

4.3. Fabrication of the Encapsulation Material

The liquid Ecoflex precursor used as encapsulation material [00–30, Smooth-On, PA, USA] was composed of 50.0 vol% A-type and 50.0 vol% B-type Ecoflex.

Supplementary Materials: The following are available online at <https://www.mdpi.com/article/10.3390/electronics10222778/s1>, Figure S1: Using laser engraving machine to make PET film with hollow circuit pattern, Figure S2: Thin film of polyethylene terephthalate (PET) with specific sensor pattern used for the fabrication of the strain sensor, Figure S3: Illustration of resistance-uniaxial tensile strain measurement, Figure S4: Characterize the relationship between resistance change and deformation of liquid metal traces on flexible substrates by using a tensile measuring instrument, Figure S5: The physical diagram and schematic diagram of the NFC tag module, Figure S6: Physical photo of the NFC reader testing platform, Figure S7: An example of the patch detecting the bending motion of the index finger and interacting with the external NFC reader.

Author Contributions: Conceptualization, S.L., J.F., T.Y., Y.T., S.D. and J.W.; methodology, S.L., J.F., T.Y., Y.T. and S.D.; software, S.L. and T.Y.; validation, S.L., J.F., T.Y. and Y.T.; formal analysis, S.L., J.F., T.Y. and Y.T.; investigation, S.L., J.F., T.Y. and Y.T.; resources, J.F., T.Y., Y.T. and S.D.; data curation, S.L. and T.Y.; writing—original draft preparation, S.L.; writing—review and editing, J.F., T.Y., Y.T., S.D. and J.W.; visualization, J.F. and T.Y.; supervision, J.W.; project administration, J.W.; funding acquisition, J.W. All authors have read and agreed to the published version of the manuscript.

Funding: This work was supported by the National Key R&D Program of China (2017YFB1002900), the National Natural Science Foundation of China (NSFC) (61775035, 61805037, 61875241, 11734005), the Natural Science Foundation of Jiangsu Province (BK20181268), and the National Natural Science Foundation of China (Grant No. 62075040).

Informed Consent Statement: Written informed consent has been obtained from the patients to publish this paper.

Data Availability Statement: The corresponding data can be obtained from the corresponding author upon proper request.

Acknowledgments: No support is provided, which is not covered by the author contribution or funding sections.

Conflicts of Interest: The authors declare no conflict of interest.

References

1. Yao, G.; Yin, C.; Wang, Q.; Zhang, T.; Chen, S.; Lu, C.; Zhao, K.; Xu, W.; Pan, T.; Gao, M.; et al. Flexible bioelectronics for physiological signals sensing and disease treatment. *J. Mater.* **2020**, *6*, 397–413. [\[CrossRef\]](#)
2. Lochner, C.M.; Khan, Y.; Pierre, A.; Arias, A.C. All-organic optoelectronic sensor for pulse oximetry. *Nat. Commun.* **2014**, *5*, 5745. [\[CrossRef\]](#) [\[PubMed\]](#)
3. Gao, W.; Emaminejad, S.; Nyein, H.Y.Y.; Challa, S.; Chen, K.; Peck, A.; Fahad, H.M.; Ota, H.; Shiraki, H.; Kiriya, D.; et al. Fully integrated wearable sensor arrays for multiplexed in situ perspiration analysis. *Nature* **2016**, *529*, 509. [\[CrossRef\]](#) [\[PubMed\]](#)
4. Sempionatto, J.R.; Lin, M.; Yin, L.; de la Paz, E.; Pei, K.; Sonsa-ard, T.; Silva, A.N.D.L.; Khorshed, A.A.; Zhang, F.; Tostado, N.; et al. An epidermal patch for the simultaneous monitoring of haemodynamic and metabolic biomarkers. *Nat. Biomed. Eng.* **2021**, *5*, 737–748. [\[CrossRef\]](#) [\[PubMed\]](#)
5. Xiang, L.; Zeng, X.; Xia, F.; Jin, W.; Liu, Y.; Hu, Y. Recent Advances in Flexible and Stretchable Sensing Systems: From the Perspective of System Integration. *ACS Nano* **2020**, *14*, 6449–6469. [\[CrossRef\]](#) [\[PubMed\]](#)
6. Hong, Y.J.; Lee, H.; Kim, J.; Lee, M.; Choi, H.J.; Hyeon, T.; Kim, D.-H. Multifunctional Wearable System that Integrates Sweat-Based Sensing and Vital-Sign Monitoring to Estimate Pre-/Post-Exercise Glucose Levels. *Adv. Funct. Mater.* **2018**, *28*, 1805754. [\[CrossRef\]](#)
7. Nyein, H.Y.Y.; Bariya, M.; Tran, B.; Ahn, C.H.; Brown, B.J.; Ji, W.; Davis, N.; Javey, A. A wearable patch for continuous analysis of thermoregulatory sweat at rest. *Nat. Commun.* **2021**, *12*, 1823. [\[CrossRef\]](#)
8. Li, C.; Cui, Y.-L.; Tian, G.-L.; Shu, Y.; Wang, X.-F.; Tian, H.; Yang, Y.; Wei, F.; Ren, T.-L. Flexible CNT-array double helices Strain Sensor with high stretchability for Motion Capture. *Sci. Rep.* **2015**, *5*, 15554. [\[CrossRef\]](#)
9. Zhou, Z.; Chen, K.; Li, X.; Zhang, S.; Wu, Y.; Zhou, Y.; Meng, K.; Sun, C.; He, Q.; Fan, W.; et al. Sign-to-speech translation using machine-learning-assisted stretchable sensor arrays. *Nat. Electron.* **2020**, *3*, 571–578. [\[CrossRef\]](#)
10. Guo, R.; Yao, S.; Sun, X.; Liu, J. Semi-liquid metal and adhesion-selection enabled rolling and transfer (SMART) printing: A general method towards fast fabrication of flexible electronics. *Sci. China-Mater.* **2019**, *62*, 982–994. [\[CrossRef\]](#)

11. Tian, H.; Shu, Y.; Cui, Y.-L.; Mi, W.-T.; Yang, Y.; Xie, D.; Ren, T.-L. Scalable fabrication of high-performance and flexible graphene strain sensors. *Nanoscale* **2014**, *6*, 699–705. [[CrossRef](#)]
12. Cai, L.; Song, L.; Luan, P.; Zhang, Q.; Zhang, N.; Gao, Q.; Zhao, D.; Zhang, X.; Tu, M.; Yang, F.; et al. Super-stretchable, Transparent Carbon Nanotube-Based Capacitive Strain Sensors for Human Motion Detection. *Sci. Rep.* **2013**, *3*, 3048. [[CrossRef](#)] [[PubMed](#)]
13. Guo, R.; Sun, X.; Yao, S.; Duan, M.; Wang, H.; Liu, J.; Deng, Z. Semi-Liquid-Metal-(Ni-EGaIn)-Based Ultraconformable Electronic Tattoo. *Adv. Mater. Technol.* **2019**, *4*, 1900183. [[CrossRef](#)]
14. Tang, J.; Zhao, X.; Li, J.; Guo, R.; Zhou, Y.; Liu, J. Gallium-Based Liquid Metal Amalgams: Transitional-State Metallic Mixtures (TransM(2)ixes) with Enhanced and Tunable Electrical, Thermal, and Mechanical Properties. *ACS Appl. Mater. Interfaces* **2017**, *9*, 35977–35987. [[CrossRef](#)] [[PubMed](#)]
15. Ozutemiz, K.B.; Wissman, J.; Ozdoganlar, O.B.; Majidi, C. EGaIn-Metal Interfacing for Liquid Metal Circuitry and Microelectronics Integration. *Adv. Mater. Interfaces* **2018**, *5*, 1701596. [[CrossRef](#)]
16. Amjadi, M.; Pichitpajongkit, A.; Lee, S.; Ryu, S.; Park, I. Highly Stretchable and Sensitive Strain Sensor Based on Silver Nanowire-Elastomer Nanocomposite. *ACS Nano* **2014**, *8*, 5154–5163. [[CrossRef](#)] [[PubMed](#)]
17. Jeong, Y.R.; Kim, J.; Xie, Z.; Xue, Y.; Won, S.M.; Lee, G.; Jin, S.W.; Hong, S.Y.; Feng, X.; Huang, Y.; et al. A skin-attachable, stretchable integrated system based on liquid GaInSn for wireless human motion monitoring with multi-site sensing capabilities. *Npg Asia Mater.* **2017**, *9*, e443. [[CrossRef](#)]
18. So, J.-H.; Dickey, M.D. Inherently aligned microfluidic electrodes composed of liquid metal. *Lab. A Chip.* **2011**, *11*, 905–911. [[CrossRef](#)]
19. Dubal, D.P.; Chodankar, N.R.; Kim, D.-H.; Gomez-Romero, P. Towards flexible solid-state supercapacitors for smart and wearable electronics. *Chem. Soc. Rev.* **2018**, *47*, 2065–2129. [[CrossRef](#)]
20. Shay, T.; Velev, O.D.; Dickey, M.D. Soft electrodes combining hydrogel and liquid metal. *Soft Matter.* **2018**, *14*, 3296–3303. [[CrossRef](#)]
21. Sharma, M.; Adalati, R.; Kumar, A.; Chawla, V.; Chandra, R. Single step fabrication of nanostructured Cr₂O₃-MoO₂ composite flexible electrode for top-notch asymmetric supercapacitor. *Appl. Surf. Sci.* **2021**, *555*, 149721. [[CrossRef](#)]
22. Chorsi, M.T.; Curry, E.J.; Chorsi, H.T.; Das, R.; Baroody, J.; Purohit, P.K.; Ilies, H.; Nguyen, T.D. Piezoelectric Biomaterials for Sensors and Actuators. *Adv. Mater.* **2019**, *31*, 1802084. [[CrossRef](#)] [[PubMed](#)]
23. Wang, Z.L.; Chen, J.; Lin, L. Progress in triboelectric nanogenerators as a new energy technology and self-powered sensors. *Energy Environ. Sci.* **2015**, *8*, 2250–2282. [[CrossRef](#)]
24. Wang, Y.; Yang, L.; Shi, X.-L.; Shi, X.; Chen, L.; Dargusch, M.S.; Zou, J.; Chen, Z.-G. Flexible Thermoelectric Materials and Generators: Challenges and Innovations. *Adv. Mater.* **2019**, *31*, 1807916. [[CrossRef](#)] [[PubMed](#)]
25. Jia, W.; Valdes-Ramirez, G.; Bandodkar, A.J.; Windmiller, J.R.; Wang, J. Epidermal Biofuel Cells: Energy Harvesting from Human Perspiration. *Angew. Chem. Int. Ed.* **2013**, *52*, 7233–7236. [[CrossRef](#)] [[PubMed](#)]
26. Park, S.I.; Brenner, D.S.; Shin, G.; Morgan, C.D.; Copits, B.A.; Chung, H.U.; Pullen, M.Y.; Noh, K.N.; Davidson, S.; Oh, S.J.; et al. Soft, stretchable, fully implantable miniaturized optoelectronic systems for wireless optogenetics. *Nat. Biotechnol.* **2015**, *33*, 1280. [[CrossRef](#)] [[PubMed](#)]
27. Lee, H.; Choi, T.K.; Lee, Y.B.; Cho, H.R.; Ghaffari, R.; Wang, L.; Choi, H.J.; Chung, T.D.; Lu, N.; Hyeon, T.; et al. A graphene-based electrochemical device with thermoresponsive microneedles for diabetes monitoring and therapy. *Nat. Nanotechnol.* **2016**, *11*, 566. [[CrossRef](#)] [[PubMed](#)]
28. Pallas-Areny, R.; Webster, J.G. *Sensors and Signal Conditioning*, 2nd ed.; John Wiley & Sons, Ltd.: Toronto, ON, Canada, 2012; pp. 73–131.